Transactions of the VSB - Technical university of Ostrava Vol. XIII, No. 1, 2018
Safety Engineering Series, ISSN 1805-3238 pp. 21 - 28, DOI 10.2478/tvsbses-2018-0004

PREPARATION OF MATERIAL BASED ON BIOCHAR - MnO_x, ITS MORPHOLOGY, THERMAL STABILITY AND PHYTOTOXICITY

Petra ROUPCOVÁ[1], Karel KLOUDA[2], Markéta WEISHEITELOVÁ[3], Bohdan FILIPI[4]

Research article

Abstract: By reducing potassium permanganate using various methods (microwave radiation, HCl, ethanol, ascorbic acid) in a biochar environment, we have prepared composites of manganese oxides and biochar as an electrode material for elements or supercapacitors. Once identified, the prepared products were tested for thermal stability and phytotoxicity as a safety parameter in case they get in contact with the natural environment. The publication had also discussed progression of thermal decomposition of the composite. The process was exo-thermal with mutual oxidation-reduction reaction between the manganese oxides and biochar carbon. In the article there are also described the adsorption capabilities of prepared products. The manganese oxide content had also influenced the phytotoxicity test results. The biochar itself had stimulating effects on all tested seeds, while composites had shown both stimulating and inhibiting effects, depending on the kind of tested seeds.

Keywords: Electrode material, composite, adsoption, thermal stability, phytotoxicity.

Introduction

The aim of this work was to prepare composite compounds of biochar-MnO_x for potential use in supercapacitors and test their thermal stability and phytotoxicity for safety reasons in case they get in contact with the natural environment. Supercapacitors (electrochemical capacitors) have been drawing a lot of attention as electrical energy storage devices as their storage density is greater than that of lithium-ion batteries or commercial capacitors. They feature the pulse charging compatibility, long life expectancy, simple principle and high discharge dynamics.

Supercapacitors are capable of absorbing high amounts of charge over very short time periods. In supercapacitors, electrical charge is stored physically (as opposed to chemically) by applying electrostatic force on the surface of electrodes at the electrode/electrolyte boundary (Lu et al., 2014). A typical supercapacitor consists of 2 electrodes, electrolyte and a separator. For so-called pseudo-capacitors (Fan et al., 2015), energy stores reversible redox by reaction on the electrode surface. The capacitors can be further sub-divided to symmetrical (same composition for all electrodes) and asymmetrical (different composition for electrodes). The basic supercapacitor concept is illustrated in Fig. 1 (Varghese et al., 2015).

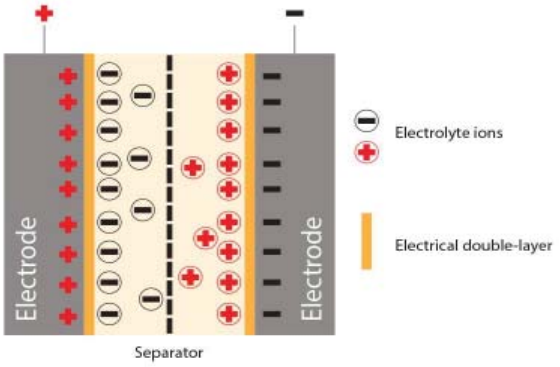

Fig. 1 Basic supercapacitor concept diagram (Varghese et al., 2015)

[1] VŠB - Technical university of Ostrava, Faculty of safety engineering, Ostrava, Czech Republic, petra.roupcova@vsb.cz
[2] VŠB - Technical university of Ostrava, Faculty of safety engineering, Ostrava, Czech Republic, karel.klouda@vsb.cz
[3] State Office for Nuclear, Chemical and Biological Protection, Milín, Czech Republic, weisheitelova@sujbcho.cz
[4] VŠB - Technical university of Ostrava, Faculty of safety engineering, Ostrava, Czech Republic, bohdan.filipi@vsb.cz

The given parameters:

These parameters are used to facilitate orientation of the examined subject.

Total capacitance in serial connection (C_T):

$$I_1 = 16,07 > 0 \quad \text{inhibition} \qquad (1)$$

C_P positive electrode capacitance,

C_N negative electrode capacitance.

Power capacity (*E*)

$$E = \frac{1}{2} C_T \cdot V^2 \qquad \text{[Wh/kg]} \ (2)$$

Power density (*P*)

$$P = \frac{V^2}{4R} \qquad \text{[W/kg]} \ (3)$$

[*V* - Element voltage; *R* - Resistance]

These values are influenced by electrode material. Nano-structural material is in the majority when we speak about electrode materials. Its surface, area, porousness and conductivity influence the contact between the electrode and electrolyte. The basic electrode material is a porous carbon material, conductive polymer and oxides of transit metals - Faraday material (including Fe_3O_4, TiO_2, NiO, MnO_2). These are electro-active materials that form electrodes for the so-called pseudo-capacitors, where the adsorption takes place via reversible redox reactions. The electrode materials applied as nano-composite MnO_x - carbonaceous materials include e.g. MnO_2 - carbonaceous nano-tubes (Chen et al., 2010; Subramanian et al., 2006), MnO_2 - graphene (Liu et al., 2010; Wang et al., 2009; Zhang et al., 2010; Zhu et al., 2011) MnO_2 - mesoporous carbon (Dong et al., 2006; Jiang et al., 2012; Zhu et al., 2005) and other porous carbonaceous material acquired via pyrolysis of natural materials (Basri and Dolah, 2013; Wei and Yushin, 2012) e.g. coconut shells, potato amyl, beer sludge, corn seeds, wood waste, bamboo, rice, coffee sediment etc.

It can also be a nano-composite of MnO_2 with conductive polymers (Meng et al., 2013; Wang et al., 2008) and a variety of combinations of MnO_2 / conductive polymer // carbon / MnO_2, / carbonaceous nanotubes / MnO_2 graphene / graphene // graphene, MnO_2 / graphene // CNT e.g. for asymmetrical capacitors (Zhai et al., 2013). For Li-ion batteries (pseudo-capacitors), a C-anode material with the following redox reaction can be used (Yan et al., 2014):

$$(MnO_2)_{solid} + M^+ + e \rightarrow MnOOM$$
$$M = Li^+, Na^+, K^+$$

Electrolytes used for applying MnO_x nano-composites include water solutions (of salts (Na_2SO_4) acids, alkalis), gel, organic or ion liquids (Varghese et al., 2015). In addition to its application as electrode materials, manganese oxide-based composite materials were applied on the C-carrier to absorb ions of arsenic, lead and copper (Zhou et al., 2017) from the water environment. Plans are being made for their application during catalytic decomposition of water into hydrogen and oxygen (Mette et al., 2012).

Material and methods

Used Chemicals

- Biochar (a product of biomass pyrolysis - Biouhel, Zlín s.r.o.) with summary formula of $C_{14}O$ containing 2 % of Si, Al, K, Ca, Mg salts;
- $KMnO_4$, HCl, C_2H_5OH, ascorbic acid (Sigma Aldrich).

Used devices

- SEM analysis: FEI Quanta 650 FEG scanning electron microscope (FEI, USA),
- TGA/DSC2 Mettler-Toledo.

Preparation of products A-E and Bs

Preparation of composites was based on the described principles of reduction of potassium permanganate using microwave radiation HCl, C_2H_5OH and ascorbic acid. For the carbonaceous carrier, we had a choice between graphene-oxide, its reduced form or a product of the so-called green economics, biochar, which we ended up choosing. In addition to the composite, we had the so-called birnessite (Wang et al., 2015) oxide prepared with layered structure with manganese valence of +3+4 by reducing the permanganate using hydrochloric acid with no biochar present.

Product A (microwave radiation)

Biochar (5 g) was put into a flask with 90 ml of distilled water and $KMnO_4$ (4 g) was added to it during intense stirring. The mixture was then stirred at laboratory temperature of microwave radiation for 5-7 min. This was followed by filtering, rinsing with distilled water and ethanol; after drying for 12 hours at 60-70 °C; the mass of the acquired product was 7.25 g (31 % of mass increment).

Product B (HCl)

4 g of $KMnO_4$ was dissolved in a flask with 60 ml of distilled water and biochar mixture (5 g) was heated up to 60 °C and 4 ml of concentrated 4 HCl were added to solution, drop-by-drop during intense stirring; the mixture was stirred for one more hour and then cooled down to laboratory temperature. This was followed by filtering and meticulous rinsing using distilled water and C_2H_5OH. The filtrate was dried for 12 hours at 60-70 °C, the mass of the resulting product was 7.29 g (31 % of mass increment).

Product C (C_2H_5OH)

5 g of biochar was mixed with a solution of 4 g of $KMnO_4$ and 90 ml of distilled water. After stirring, 80 ml of C_2H_5OH was added drop by drop. The mixture was stirred for 1 hour and then filtered, rinsed using distilled water and ethanol. The substance was then dried for 12 hours at 60-70 °C; the mass of the resulting product was 8.2 g (39 % of mass increment).

Product D (ascorbic acid)

4 g of $KMnO_4$ was dissolved in a flask with 90 ml of distilled water and biochar was added (5 g); after stirring, ascorbic acid was gradually added and the mixture was stirred in a water bath at 50-60 °C for 3 hours. This was followed by filtering, rinsing with distilled water and ethanol; after drying for at 60-70 °C; the mass of the acquired product was 7.4 g (32 % of mass increment).

Product Bs (Birnessite)

- the experiment procedure was the same as for product B, with no biochar involved.

Results and discussion

Chemical Composition of the Prepared Products and Their Morphology

The prepared product, the default biochar and the result of the so-called "blind experiment", i.e. a reduction of permanganate by hydrochloric acid with no biochar (according to literature(Varghese et al., 2015), a way to prepare the birnessite compound - Mn^{3+} - Mn^{4+}) were subjected to elementary micro-analysis (EDS); the results are shown in Tab. 1.

The analysis results show that product B has the highest manganese content, while product D has the lowest - once reduced by ascorbic acid, its manganese content is essentially 100 times lower than products A, B and C. Fig. 2 shows electronic images of products A-D with various manganese oxide configuration within the carbonaceous frame of biochar, biochar and birnessite.

Tab. 1 Elementary spectral micro-analysis of (EDS) products A-D, biochar and birnessite

Product	Mn content [% of mass]	Empirical product formulas	
		relative to Mn	relative to MnO_x
A (microwave radiation)	27.1	$C_{7,8}O_{2,4}Mn$	$C_{7,8}O_{2,4}MnO_2$
B (HCl)	39.3	$C_{4,6}O_{1,5}Mn$	$C_{9,2}Mn_2O_3$
C (C_2H_5OH)	30.6	$C_{6,4}O_{2,2}Mn$	$C_{6,4}O_{0,2}MnO_2$
D (ascorbic acid)	14.0	$C_{15,8}O_{7,5}Mn$	$C_{15,8}O_{5,5}MnO_2$
E biochar	0	$C_{14}O$	$C_{14}O$
Bs (birnessite)	61.4	Mn_3O_5	Mn_3O_5 (Mn_2O_3-MnO_2)

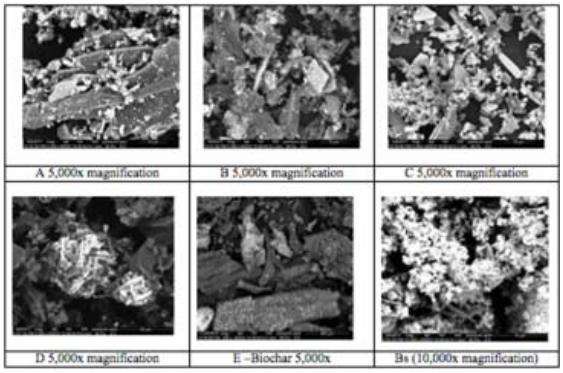

Fig. 2 Electron images of surfaces for products (A-D), biochar (E), Birnessite (Bs)

Thermal Stability of Products (A-D), Biochar (E), Birnessite (Bs)

TGA analysis (Fig. 3) was used to demonstrate the basic difference between thermal stability of products A-D, i.e. composite biochar-MnO_x, and the default biochar. Decomposition of all of the composite materials is finished at 600 °C, which is also the temperature at which the main biochar decomposition starts. Product D is the most thermally stable product of all of the tested products (see Tab. 2). Its decomposition is accompanied

by 3 exo-effects (see Fig. 6 and Tab. 2,3); unlike products A-C with 2 identified exo-effects identified. Likewise, the progression of TGA and DSC curves is similar for these products (see Fig. 3-5.) Mild endo-effects in the range of 70-80 °C are probably caused by dehydration (desorption of H_2O) with weight loss of 7-8 %. Product D only has endo-effects at 147 °C with weight loss of 2.4 %. Thermal decomposition of biochar takes place with no endo-effects. Biochar (the carbonaceous compound) had demonstrated its reducing capabilities during its reaction with potassium permanganate solution with initiation of microwave radiation, which is expected to have the following progression:

$$2KMnO_4 + 3C + H_2O \rightarrow MnO_2 + 2KHCO_3 + CO$$

One can also expect its reducing roles (Mette et al., 2012), which manifest at thermal load of the prepared composites and related reaction effects corresponding to reduction of MnO_2.

$$2MnO_2 + C \rightarrow Mn_2O_3 + CO\ (CO_2)$$

$$3MnO_3 + C \rightarrow Mn_3O_4 + CO\ (CO_2)$$

$$Mn_3O_4 + C \rightarrow 3MnO + CO$$

$$MnO + C \rightarrow MnO_x + (1\text{-}x)\ CO$$

These considerations are supported by the manganese content value comparison for the prepared products with the mass value of the sample remaining after thermal decomposition (Tab. 4). At points where x can be lesser than 1 ($x \leq 1$), one cannot exclude the possibility of creation of manganese carbide Mn_3C. The role of active carbon - biochar - was demonstrated during the so-called "blind experiment", which involves reducing a permanganate solution with no biochar present. The prepared manganese oxide (birnesitte MnO_2-Mn_2O_3) succumbed to thermal decomposition, with sample weight loss of 25 % at 1200 °C and 29 % at 1400 °C. The main weight loss (approximately 15 %) during the thermal decomposition was recorded at 40-200 °C with simultaneous endo-effect with two maximums of 68 °C and 132 °C with minimal thermal change (see Fig. 8), which probably causes morphological changes (de-oxidation, de-hydroxylation) and moisture. Further endo-effects occur at thermal maximums of 889 °C and 976 °C with minimum weight loss of 4 %. One exo-effect was identified at 477 °C with weight increment of under 1° and minimum thermal change of 155 J/g.

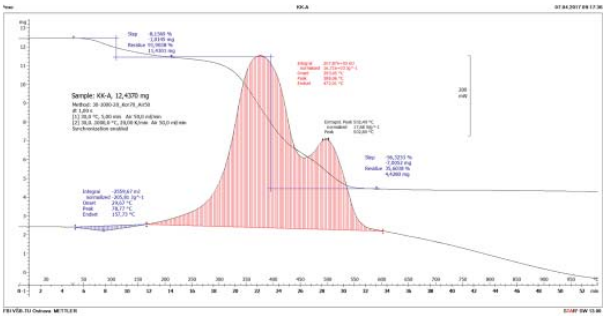

Fig. 3 TGA and DSC analysis for products A

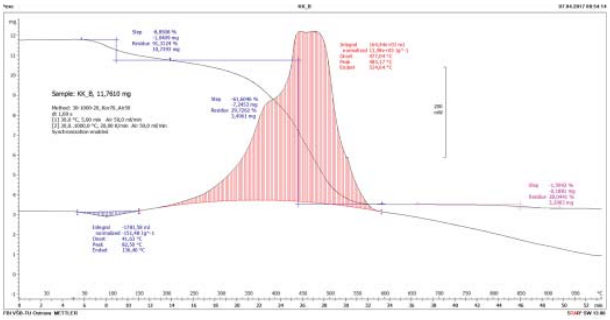

Fig. 4 TGA and DSC analysis for products B

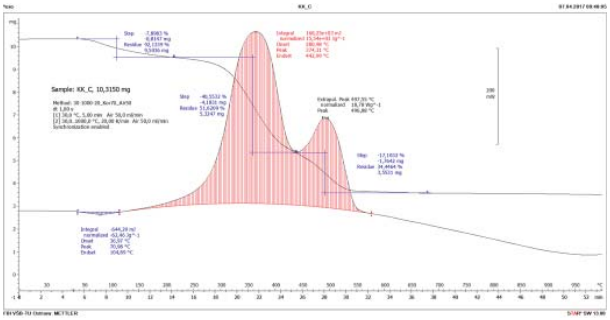

Fig. 5 TGA and DSC analysis for products C

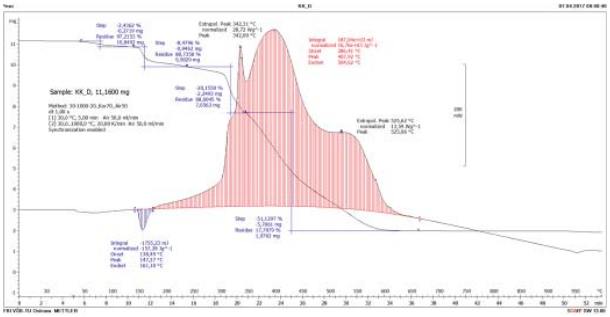

Fig. 6 TGA and DSC analysis for products D

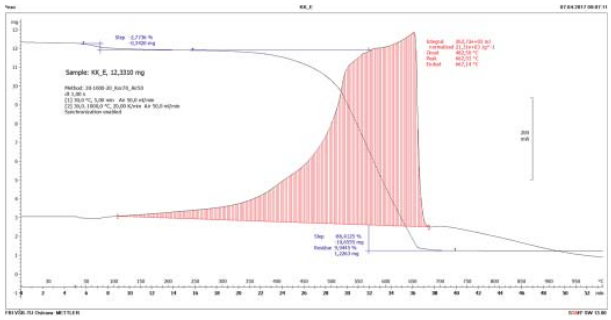

Fig. 7 TGA and DSC analysis for biochar products E

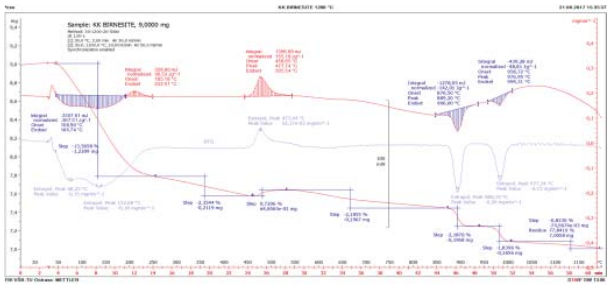

Fig. 8 TGA and DSC analysis for birnessite Bs products

Tab. 2 Beginning and ending of exo-thermal decomposition of products A-D and biochar

Product A-D and Biochar E	**A**	**B**	**C**	**D**	**E (biochar)**
Initial decomposition temperature [°C]	210	210	210	240	250
Temperature after decomposition [°C]	580	570	570	650	730

Tab. 3 Temperatures of exo-thermal effects at maximums

Product and biochar	**A**	**B**	**C**	**D**	**E**
Exo-thermal max. temperature [°C]	388 502	hint 370 485*	374 496	342 407 525	662

*continuous transition.

Tab. 4 Remaining mass of products and biochar after the decomposition

Product and biochar	**A**	**B**	**C**	**D**	**E**
Remaining mass [% of mass] after decomposition	35.6	29.7	34.5	17.7	9.9

The adsorption capabilities of prepared products

The adsorption capabilities of the prepared A-D product and biochar itself (E) respectively the permeation capabilities of the products were tested with cooperation to the SÚJCHBO v.v.i. accredited methodology on a special device for detecting resistance times of capture material against annoying substances or their substitutes "Determination of the resistance of foil materials against penetration of gas peroxide by gas chromatography, MAZL-39/10 Permeatest 4". In our case it was 1,6- dichlorhexane as a substitute for yperite.

Samples A and C essentially did not retain the substituent, for samples B and D the resistance time of 130 mg was equivalent to 81 and 83 minutes for the sample weight of 130 mg. The best results were achieved with biochar itself (E), and the resistance time was twice as large as that for samples B and D (173 minutes), testing of adsorption capabilities will be subject of further research.

Phytotoxicity

For testing of the Biochar-MnOx composite products on germinant plants, we have utilized the sensitivity of germinant seeds of mustard (*Sinapis alba L.*), lettuce (*Lactuca sativa*), garden cress (*Lepidium sativum*) and radish (*Raphanus sativus*) in their initial development stages to toxic substances (OECD Metodika 208/1984). Dosages of individual products were approximately between 0.1-0.11 g. Average root length L (in mm) is calculated from both parallel sets for each dilution, which is followed by calculating inhibition I (or stimulation) of root growth with the toxic substance in effect in comparison to the set reference sample. Root growth inhibition or stimulation is calculated using the following formula:

$$I = \frac{(L_c - L_v)}{L_c} \cdot 100 \qquad (4)$$

where:

I is the root growth inhibition or stimulation [%],

$I < 0$ ….. stimulation,

$I > 0$ ….. inhibition,

L_c is the average reference root length [mm],

L_c is the average sample root length [mm].

Example of root length calculation for product A:

$$I_1 = 16 \cdot 07 > 0 \text{ (inhibice)}$$

Fig. 9-12 shows a graphic example of placing seeds of mustard, lettuce, garden cress and radish to the proximity of the tested product A (microwave radiation). It shows that half of the samples were in direct contact with the seeds, while the other half was placed between the seeds.

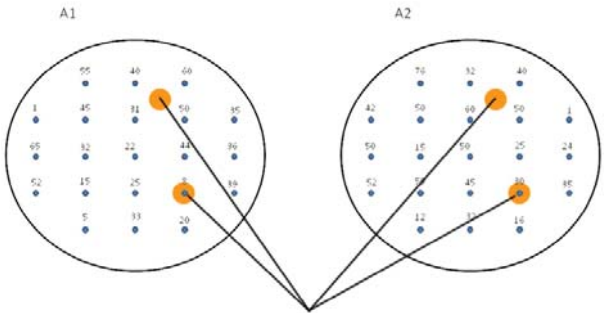

Fig. 9 Resulting mesh for product A - Biochar-MnO_x composite (white mustard)

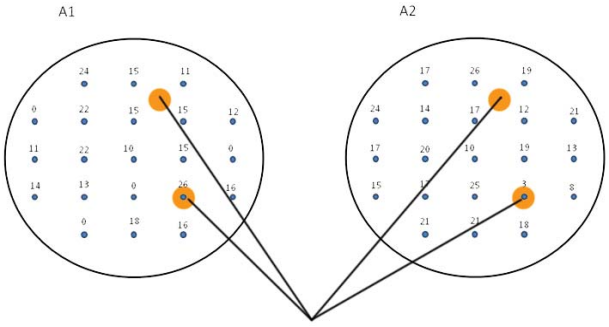

Fig. 10 Resulting mesh for product A - Biochar-MnO_x composite (lettuce)

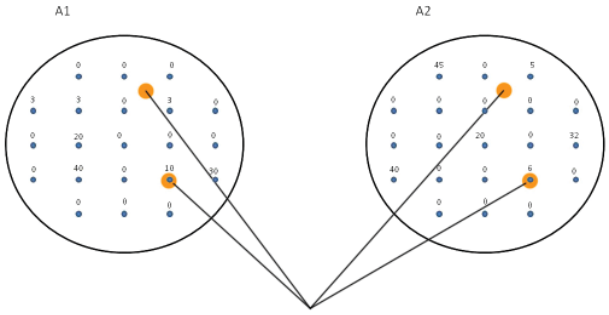

Fig. 11 Resulting mesh for product A - Biochar-MnO_x composite (garden cress)

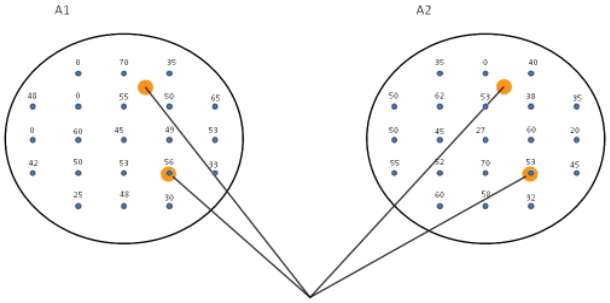

Fig. 12 Resulting mesh for product A - Biochar-MnO_x composite (radish)

Tab. 5 Summary of root length values in phytotoxicity tests for seeds of *Sinapis alba L.*

White mustard (*Sinapis alba L.*)			
Product	**Ø direct contact root length [mm]**	**Ø system root length [mm]**	***I/S**
A (microwave radiation)	19	35.71	I 16.07
B (HCl)	7.5	28.33	I 33.6
C (C_2H_5OH)	6.5	27.67	I 36.38
D (ascorbic acid)	42.5	34.21	I 19.59
E (biochar)	11.5	43.54	S -2.34

Tab. 6 Summary of root length values in phytotoxicity tests for seeds of *Lactuca sativa*

Lettuce (*Lactuca sativa*)			
Product	**Ø direct contact root length [mm]**	**Ø system root length [mm]**	***I/S**
A (microwave radiation)	14.5	15.04	S -49.06
B (HCl)	18.0	13.45	S -33.25
C (C_2H_5OH)	6.5	12.88	S -27.59
D (ascorbic acid)	8	10.3	S -2.12
E (biochar)	10.5	13.0	S -28.77

Tab. 7 Summary of root length values in phytotoxicity tests for seeds of *Lepidium sativum*

Garden cress (*Lepidium sativum*)			
Product	**Ø direct contact root length [mm]**	**Ø system root length [mm]**	***I/S**
A (microwave radiation)	8	6.12	I 6.43
B (HCl)	0	8.64	S -32.1
C (C_2H_5OH)	0	6.94	S -6.31
D (ascorbic acid)	0	9.19	S -40.53
E (biochar)	26	7.31	S -10.52

Tab. 8 Summary of root length values in phytotoxicity tests for seeds of *Raphanus sativus*

Radish (*Raphanus sativus*)			
Product	**Ø direct contact root length [mm]**	**Ø system root length [mm]**	***I/S**
A (microwave radiation)	54	43.02	I 0.86
B (HCl)	53.5	38.9	I 10.35
C (C_2H_5OH)	41.5	39.88	I 8.1
D (ascorbic acid)	59	37.31	I 14.03
E (biochar)	61	52.02	S -19.83

*I-inhibition

S-stimulation

Biochar had stimulating effects on all seeds - the greatest for lettuce and the least for mustard, see Tab. 5-8. The composites had stimulating effects on lettuce and garden cress; there was an exception for product A, with slight inhibition. White mustard had shown the highest degree of inhibition for all composites. Radish had shown greater root length in direct contact with composites than the system average. Garden cress had shown zero root growth in direct contact with products B, C, D, even though the system as a whole had been behaving in a stimulating manner.

Conclusions

Products - composites of manganese oxides with biochar - were created by reducing potassium permanganate using various agents in a biochar environment. These composites can be utilized as electrode materials for electronic elements or for capacitors. Combination of C-biochar in the presence of manganese oxides had shown in the progression of thermal decomposition. The decomposition had been progressing with exo-thermal properties and at lower temperature than the default biochar. Thermal stability of the prepared composites was lower than that of biochar or bivalent oxide - birnessite. Presence of manganese oxides also affected the phytotoxicity results, as biochar with no manganese had a stimulating effect on all tested seeds. Different behaviour of various seeds during phytotoxicity tests was shown in our case as well. Seeds of white mustard and radish (and partially garden cress) were inhibited by all products with manganese content, unlike lettuce whose root growth was stimulated.

Acknowledgements

The publication was written as a part of the Student Grant Competition "Preparation of New Carbon-based Nano-materials and their Modifications on Nano-metal Composites Using New Ways and Monitoring of Nano-material Relation to the Natural Environment" - project number SP2017/95.

References

Basri, N.H., Dolah, B.N.M. Physical and electrochemical properties of supercapacitor electrodes derived from carbon nanotube and biomass carbon. Int. J. Electrochem. Sci. 2013, 8: 257-273.

Chen, W., Fan, Z., Gu, L., Bao, X., Wang, C. 2010. Enhanced capacitance of manganese oxide via confinement inside carbon nanotubes. Chemical Communications. 46(22): 3905-3907. DOI:10.1039/C000517G.

Dong, X., Shen, W., Gu, J., Xiong, L., Zhu, Y., Li, H., Shi, J. 2006. MnO2-Embedded-in-Mesoporous-Carbon-Wall Structure for Use as Electrochemical Capacitors. The Journal of Physical Chemistry B. 110(12): 6015-6019. DOI:10.1021/jp056754n.

Fan, X., Xuli Chen, X., Dai, L. 2015. 3D graphene based materials for energy storage. Current Opinion in Colloid & Interface Science. 20(5): 429-438. DOI:10.1016/j.cocis.2015.11.005.

Jiang, H., Ma, J., Li, C. 2012. Mesoporous Carbon Incorporated Metal Oxide Nanomaterials as Supercapacitor Electrodes. Advanced Materials. 24(30): 4197-4202. DOI:10.1002/adma.201104942.

Liu, Ch., Yu, Z., Neff, D., Zhamu, A., Jang, B.Z. 2010. Graphene-Based Supercapacitor with an Ultrahigh Energy Density. Nano Letters. 10(12): 4863-4868. DOI:10.1021/nl102661q.

Lu, X., Yu, M., Wang, G., Tong, Y., Li, Y. 2014. Flexible solid-state supercapacitors: design, fabrication and applications. Energy & Environmental Science. 7(7): 2160-2181. DOI:10.1039/C4EE00960F.

Meng, F., Yan, X., Zhu, Y., Si, P. 2013. Controllable synthesis of MnO_2/polyaniline nanocomposite and its electrochemical capacitive property. Nanoscale Research Letters. 8(1): 179. DOI:10.1186/1556-276X-8-179.

Mette, K., Bergmann, A., Tessonnier, J-P., Hävecker, M., Yao, L., Ressler, T., Schlögl, R., Strasser, P., Behrens, M. 2012. Nanostructured Manganese Oxide Supported on Carbon Nanotubes for Electrocatalytic Water Splitting. ChemCatChem. 4(6): 851-862. DOI:10.1002/cctc.201100434.

Subramanian, V., Zhu, H., Wei, B. 2006. Synthesis and electrochemical characterizations of amorphous manganese oxide and single walled carbon nanotube composites as supercapacitor electrode materials. Electrochemistry Communications. 8(5): 827-832. DOI:10.1016/j.elecom.2006.02.027.

Varghese, Seba S., Lonkar, S., Singh, K.K., Swaminathan, S., Abdala, A. 2015. Recent advances in graphene based gas sensors. Sensors and Actuators B: Chemical. 218: 160-183. DOI:10.1016/j.snb.2015.04.062.

Wang, Y., Shi, Z., Huang, Y., Ma, Y., Wang, C., Chen, M., Chen, Y. 2009. Supercapacitor Devices Based on Graphene Materials. The Journal of Physical Chemistry C. 113(30): 13103-13107. DOI:10.1021/jp902214f.

Wang, S., Gao, B., Li, Y., Mosa, A., Zimmerman, A.R., Ma, L.Q., Harris, W.G., Migliaccio, K.W., 2015. Manganese oxide-modified biochars: Preparation, characterization, and sorption of arsenate and lead. Bioresour. Technol. 181: 13-17. DOI:10.1016j.biortech.2015.01.044.

Wang, Y-G., Wu,W., Cheng, L., He, P., Wang, C-X., Xia, Y-Y. 2008. A Polyaniline Intercalated Layered Manganese Oxide Nanocomposite Prepared by an Inorganic/Organic Interface Reaction and Its High Electrochemical Performance for Li Storage. Advanced Materials 20. DOI:10.1002/adma.200701708.

Wei, L., Yushin, G. Nanostructured activated carbons from natural precursors for electrical double layer capacitors. 2012. Nano Energy. 1(4): 552-565. DOI:10.1016/j.nanoen.2012.05.002.

Yan, J., Wang, Q., Wei, T., Fan, Z. 2014. Recent Advances in Design and Fabrication of Electrochemical Supercapacitors with High Energy Densities. Advanced Energy Materials. 4(4): DOI:10.1002/aenm.201300816.

Zhai, T., Wang, F., Yu, M., Xie, S., Liang, C., Li, C., Xiao, F., Tang, R., Wu, Q., Lu, X., Tong, Y. 2015. 3D MnO_2-graphene composites with large areal capacitance for high-performance asymmetric supercapacitors. Nanoscale. 5(15): 6790-6796. DOI:10.1039/C3NR01589K.

Zhang, L.L., Zhou, R., Zhao, X.S. 2010. Graphene-based materials as supercapacitor electrodes. Journal of Materials Chemistry. 20(29): 5983-5992. DOI:10.1039/C000417K.

Zhou, L., Huang, Y., Qiu, W., Sun, Z., Liu, Z., Song, Z. 2017. Adsorption Properties of Nano-MnO_2-Biochar Composites for Copper in Aqueous Solution. Molecules. 22(1): 173. DOI:10.3390/molecules22010173.

Zhu, S., Zhou, H., Hibino, M., Honma, I., Ichihara, M. 2005. Synthesis of MnO_2 Nanoparticles Confined in Ordered Mesoporous Carbon Using a Sonochemical Method. Advanced Functional Materials. 15(3): 381-386. DOI:10.1002/adfm.200400222.

Zhu, Y., Murali, S., Stoller, M.D., Ganesh, K.J., Cai, W., Ferreira, P.J., Pirkle, A., Wallace, R.M., Cychozs, K.A., Thomess, M., Su, D., Stach, E. A., Ruoff, R.S. 2011. Carbon-Based Supercapacitors Produced by Activation of Graphene. Science. 332(6037): 1537-1541. DOI:10.1126/science.1200770.